Fundamental aspects of phase formation in WC-based cemented carbides containing FeMn-based binders

R. de Oro Calderon [a,*], M. Lunzer [b], I. Wodak [a], R. Steinlechner [a]

[a] *TU Wien, Vienna 1060, Austria*
[b] *Boehlerit GmbH & Co KG, Kapfenberg 8605, Austria*

ABSTRACT

The hardmetal industry is continuously seeking for (Co, Ni)-free binder alternatives. Several attempts have been made to use Fe—Mn binders, Mn being a very effective austenite stabilizer. Substitution of Co binders for Fe—Mn based binders comes along with many challenges such as: narrow carbon windows, evaporation of Mn during sintering or the formation of stable Mn-oxides. This work presents an overview on the phase formation in hardmetals with different carbon contents prepared from FeMn, FeMnSi and FeMnNi binders. Due to the efficient role of Mn as cementite stabilizer, it was not possible to avoid the presence of eta-carbides and cementite under the conditions studied, and samples with intermediate carbon contents presented both eta-carbides and cementite in the microstructure. Only after the addition of 25 wt% of Ni to the binder it was possible to observe materials with two phase microstructures. The challenges related to Mn evaporation and formation of stable oxides can be overcome by a proper selection of the starting materials and the sintering conditions. It is thus proved that the main challenge posed by these materials is the difficulty to obtain microstructures without detrimental phases.

1. Introduction

Hardmetals based on WC-Co present excellent combinations of hardness and toughness that make them the most suitable material for most tooling applications. However, exposure to fine Co powder, in particular when combined with WC, has been associated with lung diseases among employees in the hardmetal industry, and recent studies on its carcinogenic character have motivated a reclassification by REACH [1]. Furthermore, with the growing perspectives in the electro-mobility sector, Co supply is also a major concern, especially if considering the need to mine this element in conflict regions like DR of the Congo.

The possibility of using iron and nickel as alternative binder elements in cemented carbide production was already considered in the original patent from K. Schröter in 1923 [2]. However, further developments on this family of materials were mainly focused on cobalt-based binders due to the superiority in properties [3]. In the late 1970s/early 1980s Leo Prakash made some pioneer investigations in iron-based binders, showing their advantages as compared to pure cobalt for some specific applications. He discovered, that replacing cobalt with iron-nickel-cobalt alloys could lead to hard metals with widely varying strength

properties as a result of precipitation hardening mechanisms, phase transformations, and order/disorder reactions [4]. This invention enabled the commercialization of a (7:2:1) FeNiCo binder which is still used for wear parts and woodwork applications. In 2015 Schubert et al. [5] made a thorough study on hardness, toughness, strength, wear resistance, hot hardness and creep in Fe-based binders, in particular FeNi, FeNiCo, and FeMn. In their study they also considered the analysis of the theoretical and experimental carbon windows, which is of outmost importance for the industrial implementation. The authors report that FeNi (85/20) and FeNiCo (70/20/10) binders show, at room temperature, excellent combinations of hardness and toughness even as compared to industrial WC-Co alloys. However, the carbon windows are extremely narrow for an industrial implementation, which limits their use to materials with large binder contents. Furthermore, due to the low solubility of W in the binder phase, the high temperature properties of these materials are inferior to cobalt-based materials, which proves that a good combination of hardness-toughness does not necessarily provide a good metal-cutting performance. On the other hand, FeNiCo (40/40/20) exhibited a significantly broader carbon window due to the higher additions of Co and Ni, and presented a stable austenitic metallic binder, which rendered this alloy as the most promising alternative to Co-based

materials, from an industrial perspective. However, the properties evaluated in this study were considerably inferior to those of WC-Co alloys processed under similar conditions. The authors conclude that a substitution of Co by FeNiCo (40/40/20) in metal-cutting are viable, but the properties at room temperatures and at high temperatures are, at the lab scale, clearly inferior. Further information on application testing would be necessary for these materials.

A completely Co- and Ni-free alternative to WC-Co materials are cemented carbides with FeMn-based binders. Manganese stabilizes the austenitic phase of iron, which is also the phase present in conventional WC-Co carbides. Austenite is known to be more ductile than ferrite, thus good toughness properties could be expected. Mn is among the most effective alloying elements for steels [6], and the properties of Mn containing steels can be significantly improved by the so-called TRIP effect (transformation induced plasticity), or with higher manganese contents by the TWIP effect (twinning induced plasticity) [7–9]. A very special family of Mn steels are the so-called "Hadfield steels", which typically contain around 10–15 wt% Mn and 0.8–1.25 wt% C. These type of austenitic steels are soft as-quenched but present excellent work hardening capability while retaining their toughness [10–13].

A patent from 1982 reports the successful use of Fe-14Mn-5Ni as substitutes of Co during machining (turning tests). The authors observed, for materials containing 6 wt% and 10 wt% binder, similar performances for Fe-based binders as for the equivalent Co-based materials. The patent reports the use of a water-quenching process to give the desired product [14].

In 1983 the use of FeMn binders in hardmetals was systematically analyzed by Leo Prakash [15,16], who considered Mn additions in the range 5–16 wt% for hardmetals with 20 wt% binder. The author reports an entirely ferritic binder phase at 6 wt% Mn and fully austenitic binder at 16 wt% binder. The hardmetals produced showed lower toughness and transverse rupture strength than WC-Co, but significantly improved hardness, hot hardness and abrasive wear resistance.

Wittmann and Schubert [5,17] also report studies on WC-10 wt% FeMn hardmetals. Significant manganese losses by evaporation lead to binders that were mostly ferritic. By optimizing the sintering conditions the authors could produce hardmetals with binders that contained up to 16 wt% Mn. For these materials the authors report high values of hardness but again rather poor toughness.

The TRIP effect in Fe-22 wt% Mn binders was confirmed by Maccio et al. [18] on wear surfaces that had been considerably work-hardened. However, at the carbon contents studied, the materials produced always contained either eta-carbides or cementite.

Hanyaloglu et al. [19] studied materials containing 15 wt% and 25 wt% binder, with a binder composition Fe-13.5 wt%Mn. Again hardness values reported are high, but toughness is lower as compared to WC-Co references. The authors highlight the need of using carburizing atmospheres in order to retain sufficient carbon in the material and thus avoid formation of eta-carbides.

Maccio Colmenares [20] presents a systematic study on Fe—22Mn and Fe-22Mn-3.4Si binders supported on thermodynamic calculations, and using prealloyed powders with the desired binder composition. Even though the oxygen content of the prealloyed particles was rather low (0.02 wt%) a massive presence of oxides was observed after sintering under protective atmospheres (Ar or N$_2$), especially in alloys containing Si. The samples always contained either eta-carbides or cementite, depending on the total carbon content, and the authors point out the need of finding the optimum carbon contents that can avoid the presence of a third phase.

Both Prakash [16] and Wittmann [17] investigated the crystal structure of the binder phase, but at different binder contents, of 20 and 10 wt% respectively. While Prakash reports that from a Mn content of 16 wt% almost exclusively austenite is present, Wittmann shows that at this composition still mainly ferrite is present. Maccio reports a completely austenitic microstructure at 22 wt% Mn for binder additions of 20 wt% [20]. Hanyaloglu [19] also reports a purely austenitic binder

at 13.5 wt% Mn, while Tarraste was still able to detect ferrite phase at 20 wt% Mn, although both used a binder content of 15 wt% [21]. In summary, there is no consistent picture of the extent to which manganese stabilizes the austenitic phase.

An important aspect when considering the use of Mn-containing binders is the risk of Mn losses during sintering, due to the relatively high vapor pressure of Mn already at temperatures around 900 °C. Mn alloying in sintered steels has been thoroughly studied by Andrej Šalak [22–28] who describes challenges such as the high oxygen affinity of Mn, and the Mn sublimation at relatively low temperature, but he also presents some strategies to advantageously use some of this phenomena to improve the properties of Mn-containing materials (e.g. the "self-cleaning" effect of Mn vapours that can get the oxidizing species from the atmosphere before they reach the specimen). Wittmann [17] reports Mn losses of up to 85% in cemented carbides, and proposes suitable methods to retain Mn in the material such as: the reduction of the sintering temperatures, the use of an Ar-or N$_2$-pressure of ~10 mbar (or even higher) or the creation of a manganese vapor "microatmosphere" in the sintering device by surrounding the samples with manganese metal or ferromanganese. Under optimized sintering conditions, the authors retained up to 16 wt% Mn in the binder.

In summary, there are a number of aspects regarding the use of (Co, Ni)-free FeMn-based binders that still need to be understood. The present work investigates in detail the phase formation in FeMn- based binders at different carbon contents, as well as the possible addition of further alloying elements to the binder (Si and Ni) that can broaden the experimentally observed carbon windows. The present study is based on a combination of thermodynamic calculations and experiments and intends to provide a better overview on the constitution and composition of these materials. In this work, Mn was introduced by using FeMn masteralloy powders. The powders were produced using a novel technique named "Ultra High Pressure Water Atomization" [29] which allows obtaining high yields of particles with mean sizes around 6 μm. In contrast to conventional gas atomized powders for which the mean size is around 20 μm, these powders present a more favorable particle size distribution in particular for their use in hardmetals production.
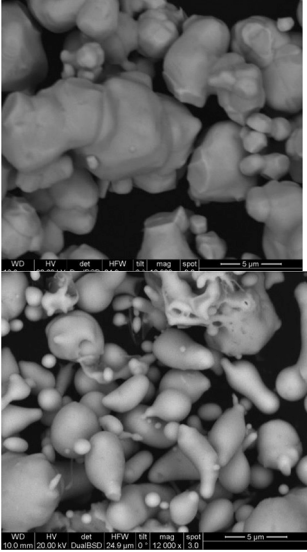
2. Experimental procedure

Five different alternative binders were analyzed in this study, namely: Fe16Mn, Fe16Mn1Si, Fe16Mn4Si, Fe25Mn11Ni and Fe22.5Mn25Ni. Thermodynamic calculations were used to evaluate the carbon window expected for each binder composition considering mixes containing WC + 20 wt% Binder. ThermoCalc and the commercially available database TCFE9 were used for this purpose. At least 4 different carbon contents were evaluated for each binder family. At the lowest carbon contents eta-carbides were expected, while at the highest carbon contents graphite/cementite was expected.

PM standard grade elementary powders (Fe-carbonyl, Ni, W, carbon black) were used for the preparation of the different alloys. In order to introduce the required amounts of Mn and Si, Fe-based masteralloy powders produced by Ultra High Pressure Water Atomization (UHPWA-Atomizing Systems Ltd. UK) were used, and admixed (when needed) with Fe carbonyl powder to adjust the binder composition. The characteristics of the WC and masteralloy powders used in this study are presented in Table 1.

For the preparation of the powder batches, the respective powders were mixed for 2 h in a Turbula mixer without wax. The coarse and rounded morphology of the WC powders provided a good mixing quality and homogeneous microstructures after sintering. The green parts were uniaxially pressed at 200 MPa. The parts were then sintered in a N$_2$—10H$_2$ atmosphere at temperatures between 1300 °C–1380 °C depending on the binder composition. Heating and cooling rates were 15 °C/min in the sintering furnace. Selected samples were –after sintering- quenched in a Linseis quenching dilatometer by heating at 1370 °C (heating rate ~ 200 °C/s) and cooling at 100 °C/s.

Table 1
Characteristics of the WC and masteralloy powders used in this study.

WC powder	Starting high purity WC powder FSSS particle size: 5.4 µm (de-agglomerated). Total carbon: 6.13 wt %. Producer: WBH, Austria
Masteralloy powders	Compositions: MA1: Fe-53Mn-3.7C MA2: Fe-33Mn-7.5Si-0.3C Oxygen content ~0.2 wt% (determined via carrier gas melt extraction using a LECO TC400 device) Particle size distribution: d_{10} ~ 2 µm; d_{50}: 6 µm; d_{90}: 15 µm (Laser Diffraction Equipment CILAS 920 Liquido) Producer: Atomizing Systems Ltd. UK

Sample cross sections were characterized using optical microscopy (with an Olympus GX51 microscope) as well as Scanning Electron Microscopy (SEM) FEI QUANTA 200 ESEM. Energy-Dispersive X-ray Spectrometry (EDS) was used as a semi-quantitative method to measure the chemical composition in different binder pools. Both point analysis and element mapping identification in selected areas were taken for this purpose. X-Ray Diffraction (XRD) was used to identify the phases present in the "as-sintered" alloy (after metallographic preparation and stress-relieve polishing, but before etching), using a PANalytical X'Pert PRO diffractometer (Cu Kα1 radiation). Selective etching of phases on the sample cross section was performed by using different reactants in order to improve the evaluation of phase formation.

3. Results

3.1. Thermodynamic calculations

Fig. 1 presents the calculated isopleths (T vs wt%C) for WC-based cemented carbides with 20 wt% of different binder phases. One of the important challenges when using Fe-based binders can be clearly recognized from phase diagrams such as the one shown in Fig. 1-a (for WC-20 wt% Fe). As it was already reported by Guillermet [30–32], Fe-binders present a rather narrow two phase region (the region where only WC and metallic fcc binder are stable) particularly due to the so called "roofing": a certain region of the two phase area is covered by a region- at higher temperatures- in which eta-carbides are stable. In that range of compositions, eta-carbides may precipitate during cooling and remain present in the microstructure as metastable phases at room temperature. The diagram in Fig. 1-a is calculated for 20 wt% binder, if the amount of binder decreases, the carbon window would be further reduced, which makes the use of Fe-rich binders rather unrealistic from an industrial perspective. For a Mn-containing binder (Fe16Mn in Fig. 1-b) the diagram looks very similar. However, due to the effective role of Mn as cementite stabilizer [33], with Fe16Mn binders, on the right side of the carbon window (i.e. at high carbon contents) cementite is stabilized instead of graphite.

Fig. 1 c) and d) show the effect of adding different amounts of Si to the Fe16Mn binder: 1 wt% in c) and 4 wt% in d). According to the diagrams, increasing amounts of Si in the binder tend to broaden the effective carbon window, and to stabilize graphite instead of cementite at the higher carbon contents. No additional phases are predicted for these two systems.

Additions of Ni to the FeMn binder were also evaluated. Different combinations of Fe, Mn and Ni were investigated, considering only Ni additions below 25 wt%. The diagrams presented in Fig. 1 e) and f) show the results for two of the systems studied: Fe25Mn11Ni and Fe22.5Mn25Ni. According to the calculations, the addition of Ni does not provide a clear advantage in terms of broadening the 2-phase region, however, increasing additions of Ni tend to promote the stabilization of graphite (instead of cementite) at high carbon contents.

3.2. Constitution, composition and hardness of the alloys studied

Table 2 presents a summary of the results obtained for all of the alloys analyzed in this study, both in the calculations as in the experiments. The table indicates the nominal carbon content of each one of the mixes prepared. The final carbon content would depend on the carbon losses during sintering and would therefore be dependent on the sintering conditions. In this study, the main focus was placed in obtaining alloys located all along the carbon window and, for this reason, the nominal carbon content is used as reference value. The table shows the stable phases as calculated with ThermoCalc at 1000 °C (temperature at which the microstructure is considered to freeze during the sintering process). Additionally, the expected binder composition of the binder phase at this temperature is also presented on the table. Experimental values are also included in Table 2. The experimentally observed phases as declared in Table 2 were detected using a combination of techniques: selective etching, XRD and SEM + EDS mappings/point analyses, as described in in [34,35]. The results presented in Table 2 are described in detail in the forthcoming sections.

3.2.1. Phase formation in alloys containing Fe16Mn binders

Fig. 2 illustrates the isopleth for WC-20(Fe16Mn) indicating the nominal carbon contents considered in this study, and including also the microstructure of the respective samples after etching with Murakami reagent for 3 s. Most of the samples prepared showed eta-carbides. With increasing nominal carbon contents the amount of eta-carbides decreases, and tend to present a dendritic morphology (see samples with 5.3 wt%C) which might indicate that the sample was located within the "roofed" region of the diagram. Neither eta-carbides nor graphite were observed in the samples containing 5.6 wt%C. In this sample, however, the presence of cementite is evidenced both from the etched microstructure and from XRD analysis (see Fig. 3-right). What is particularly interesting in this family of alloys is the fact that, in the sample with 5.3 wt%C, not only eta-carbides are observed but also cementite is revealed both in the selectively etched microstructure and in the XRD pattern (see Fig. 3-left). The simultaneous presence of eta-carbides and cementite in the 5.3 wt%C sample suggests that -at least under the sintering conditions studied- there is no effective carbon window in this system, and the presence of either eta-carbides, or cementite, or both, cannot be avoided.

The use of fast cooling rates might prevent the formation of eta-carbides, in samples located within the "roofed" area [36]. In order to investigate this effect, a small part of the samples showed in Fig. 2 was re-heated inductively in a quenching dilatometer up to 1370 °C (heating rate approximately 200 °C/s) and then rapidly cooled up to room temperature at approximately 100 °C/s. Such high cooling rates proved to be efficient for avoiding the formation of eta-carbides on cooling in samples containing 5.3 wt% C (see Fig. 4). In case of samples with 5.6 wt % C the microstructure might suggest the presence of graphite. However, the porosity observed in these samples was not related to the presence of graphite, but it is a consequence of the experimental set-up.
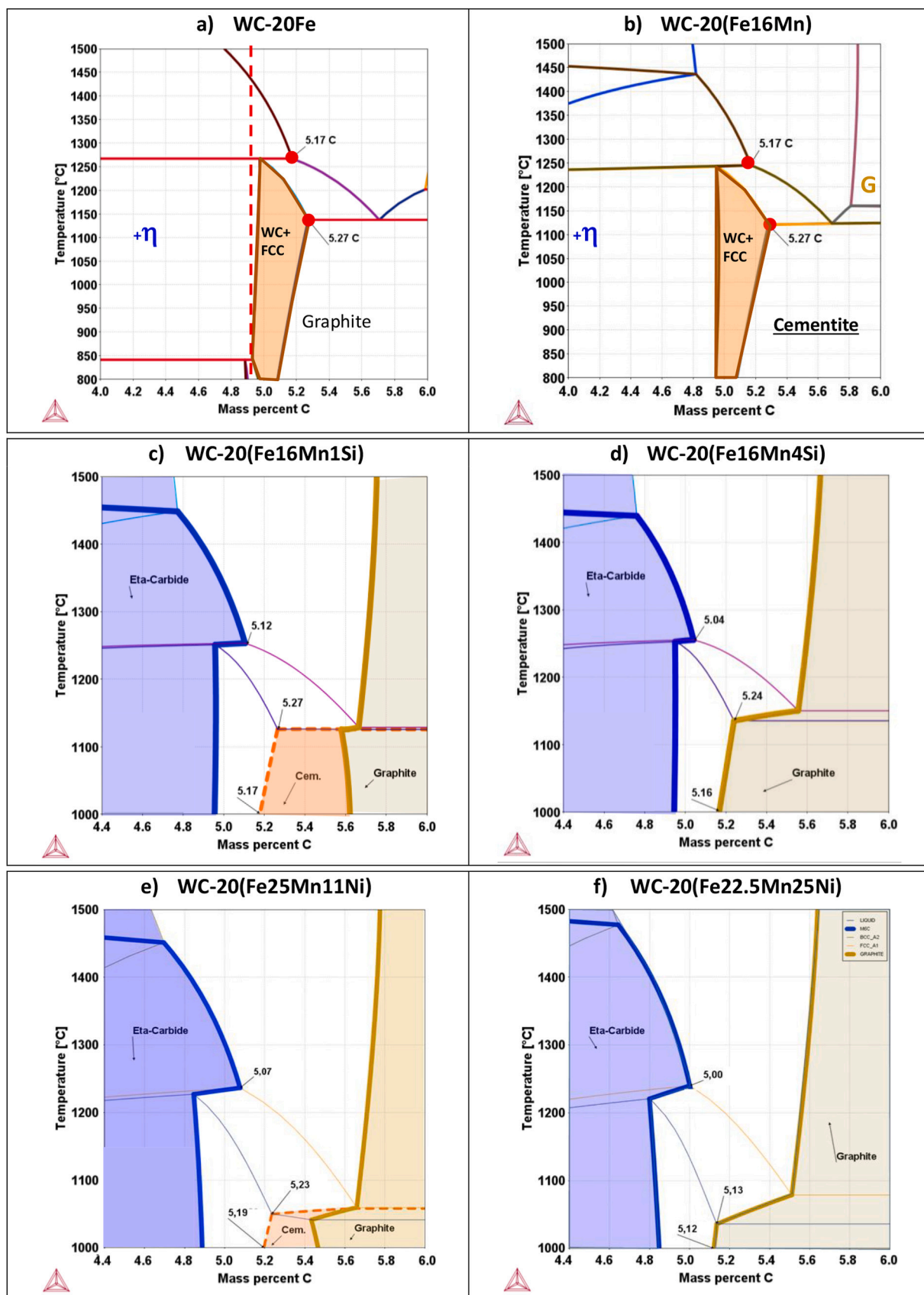
Fig. 1. Isopleths (T vs wt%C) for WC-based cemented carbides containing 20 wt% of different binder systems. Calculated with the software ThermoCalc and the database TCFE9

Table 2
Theoretical and experimental information on phase formation and solubilities in the binder phase for the different alloys studied. HV30 values for selected alloys.

Binder	Nom. C (wt%)	Sint. T.(°C)	Calculations (1000 °C)		Experimental		
			Stable Phases	Binder composition (wt%)	Stable Phases	Binder composition (wt%)	HV30
Fe16Mn	4.6	1300	WC, FCC, η	Fe-17.5Mn-5.9 W-0.6C	WC, FCC, η	Fe-15.5Mn-4.0 W	979
	5.1		WC, FCC	Fe-15.4Mn-2.7 W-1.2C	WC, FCC, η	Fe-15.3Mn-3.7 W	844
	5.3		WC, FCC, Fe$_3$C	Fe-14.5Mn-1.9 W-1.6C	WC, FCC, η, Fe$_3$C	Fe-15.8Mn-3.5 W	872
	5.6		WC, FCC, Fe$_3$C	Fe-12.2Mn-1.7 W-1.6C	WC, FCC, Fe$_3$C	Fe-14.6Mn-2.7 W	912
Fe16Mn-q Q ~ 100 K/s	4.6	–	–	–	WC, FCC, η	Fe-14Mn-10 W	1013
	5.1				WC, FCC, η, Fe$_3$C	Fe-13.2Mn-9.8 W	909
	5.3				WC, FCC, Fe$_3$C	Fe-13.1Mn-9.8 W	859
	5.6				WC, FCC, Fe$_3$C	Fe-12.2Mn-8.1 W	876
Fe16Mn1Si	4.8	1380	WC, FCC, η	Fe-15.9Mn-1.0Si-4.0 W-0.4C	WC, FCC, η	Fe-14.5Mn-0.6Si-4.0 W	934
	5.0		WC, FCC	Fe-15.3Mn-1.0Si-2.5 W-0.7C	WC, FCC, η	Fe-15.7Mn-0.9Si-3.9 W	827
	5.1		WC, FCC	Fe-15.4Mn-1.0Si-1.6 W-1.2C	WC, FCC, η	Fe-15.4Mn-0.9Si-4.4 W	865
	5.3		WC, FCC, Fe$_3$C	Fe-14.4Mn-1.1Si-1.1 W-1.4C	WC, FCC, η, Fe$_3$C	Fe-14.9Mn-1.0Si-3.6 W	856
Fe16Mn4Si	4.8	1300	WC, FCC, η	Fe-16.4Mn-4.0Si-1.9 W-0.2C	WC, FCC, BCC, η	Fe-17.1Mn2.9Si-3.5 W	911
	5.0		WC, FCC	Fe-15.8Mn-3.9Si-0.7 W-0.5C	WC, FCC, BCC, η, M$_5$Si$_3$	Fe-17.3Mn-3.5Si-2.6 W	877
	5.1		WC, FCC	Fe-15.8Mn-3.9Si-0.4 W-1.0C	WC, FCC, BCC, η, M$_5$Si$_3$	Fe-17.7Mn-3.7Si-2.4 W	870
	5.3		WC, FCC, Graph.	Fe-15.7Mn-3.9Si-0.3 W-1.1C	WC, FCC, BCC, M$_5$Si$_3$	Fe-16.1Mn-3.6Si-1.6 W	952
Fe25Mn11Ni	4.9	1360	WC, FCC, η	Fe-23.2Mn-10.2Ni-6.8 W-0.4C	WC, FCC, η		
	5.2		WC, FCC, Fe$_3$C	Fe-24.1Mn-10.6Ni-1.9 W-0.2C	WC, FCC, η		
	5.3		WC, FCC, Fe$_3$C	Fe-23.2Mn-11.6Ni-1.7 W-1.6C	WC, FCC, η	–	–
	5.35		WC, FCC, Fe$_3$C	Fe-22.8Mn-12.1Ni-1.7 W-1.6C	WC, FCC, Fe$_3$C		
	5.4		WC, FCC, Fe$_3$C	Fe-22.4Mn-12.7Ni-1.6 W-1.6C	WC, FCC, Fe$_3$C		
	5.6		WC, FCC, Fe$_3$C	Fe-21.0Mn-15.6Ni-1.4 W-1.5C	WC, FCC, Fe$_3$C		
Fe22.5Mn25Ni	4.9	1360	WC, FCC	Fe-21.4Mn-23.7Ni-4.7 W-0.3C	WC, FCC, η	Fe-22.4Mn-24.7Ni-2.6 W	686
	5.2		WC, FCC, Graph.	Fe-21.9Mn-24.4Ni-1.1 W-1.3C	WC, FCC, η	Fe-22.1Mn-23.9Ni-1.4 W	704
	5.3		WC, FCC, Graph.	Fe-21.9Mn-24.4Ni-1.1 W-1.3C	WC, FCC	Fe-22.0Mn-24.0Ni-1.1 W	722
	5.35		WC, FCC, Graph.	Fe-21.9Mn-24.4Ni-1.1 W-1.3C	WC, FCC, Fe$_3$C	Fe-21.9Mn-23.9Ni-0.9 W	729
	5.4		WC, FCC, Graph.	Fe-21.9Mn-24.4Ni-1.1 W-1.3C	WC, FCC, Fe$_3$C	Fe-21.4Mn-24.0Ni-0.8 W	745
	5.6		WC, FCC, Graph.	Fe-21.9Mn-24.4Ni-1.1 W-1.3C	WC, FCC, Fe$_3$C, Graph.	–	–
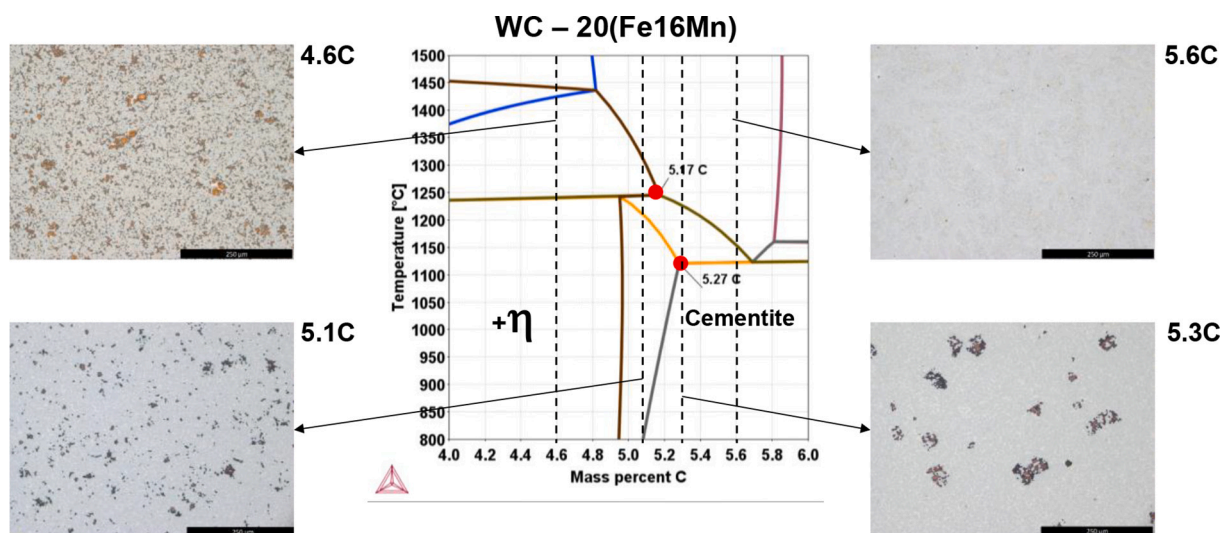
Fig. 2. Alloys WC-20 wt%(Fe16Mn) binder: Theoretical phase diagram and microstructures observed experimentally at different nominal carbon contents. Etching: Murakami.

In the quenching dilatometer the samples are held by two pushing rods that apply a certain pressure on both sides. The maximum temperature of the experiment is rather high, and, when the liquid phase is formed, the samples bend and show this type of porosity at least on one side of the sample.

In the quenched samples containing 5.3 wt%C (see Fig. 5-left), cementite cannot be detected on the XRD patters, but the selectively etched microstructures present some carbide phases that are most likely remaining cementite (as the original sample did contain cementite). Also in the case of samples wit 5.6 wt%C the amount of cementite observed both in the XRD patterns and in the metallographic sections (see Fig. 5-right) is considerably reduced as compared with the original sample with 5.6 wt%C (Fig. 3-right).

3.2.2. Phase formation in Fe16Mn1Si and Fe16Mn4Si binders

The microstructures of samples containing FeMnSi binders, after etching with Murakami reagent for 3 s, can be observed in Fig. 6. eta-carbides are present in all of the alloys prepared using Fe16Mn1Si binders, while the alloy with an Fe16Mn4Si binder did not show any eta-carbides in samples containing 5.3 wt%C (the highest carbon content considered for this family of binders). As previously described for Fe16Mn binders, with increasing nominal carbon contents a clear decrease in the amount of eta-carbides is observed (as it is to be expected), and the eta-carbides tend to present a more dendritic morphology.

Further evaluation of the alloy containing Fe16Mn1Si binder with 5.3 wt% reveals that this sample also shows a coexistence of eta-carbides
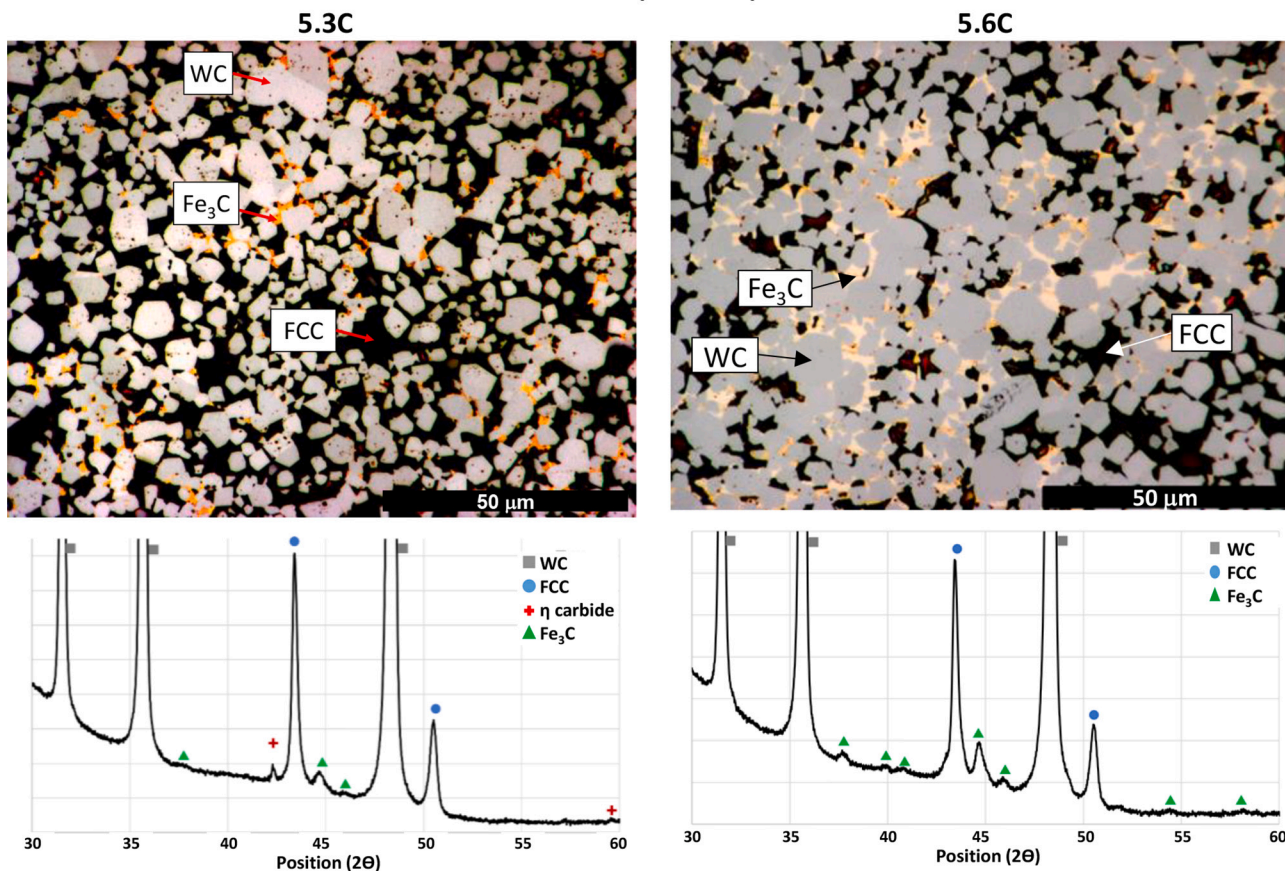
Fig. 3. Alloys WC-20 wt%(Fe16Mn) binder with nominal carbon contents 5.3 wt% C and 5.6 wt%C. X-Ray diffraction patterns and detail of the microstructure after acidic etching with diluted ferric chloride (FeCl$_3$, 5 min.).
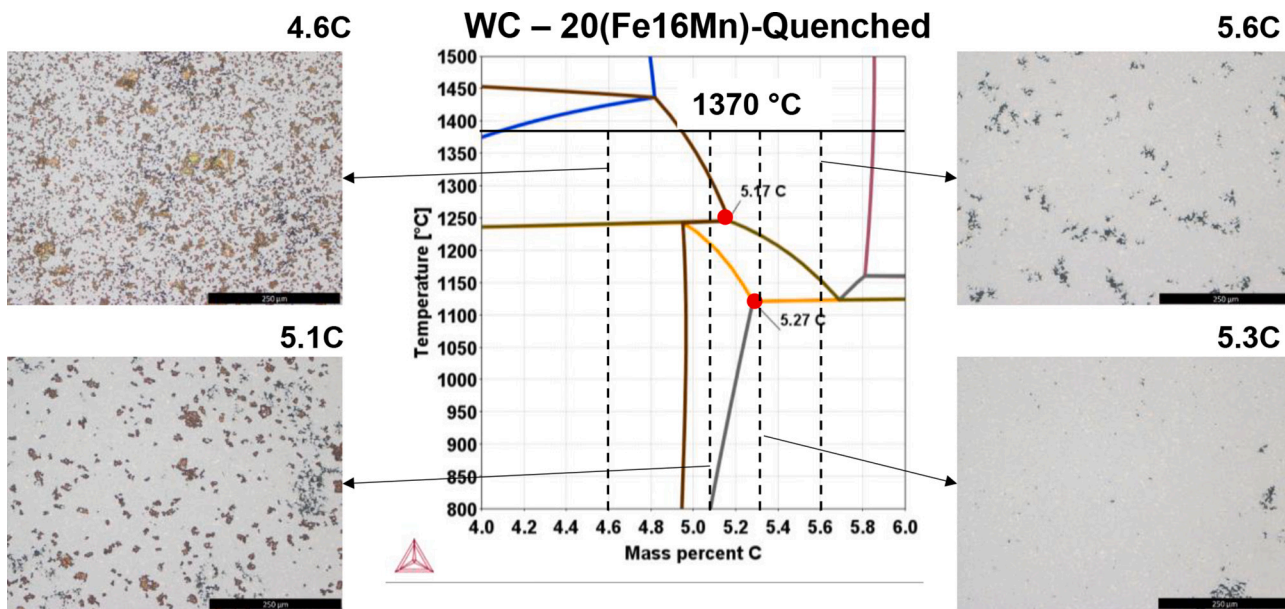

Fig. 4. Alloys WC-20 wt%(Fe16Mn) binder after quenching at ~100 °C/s from 1370 °C: Theoretical phase diagram and microstructures observed experimentally at different nominal carbon contents. Etching: Murakami.

and cementite in the microstructure, the presence of cementite again being confirmed both by selective etching of the binder phase, and by XRD analysis (see Fig. 7).

In the case of alloys containing Fe16Mn4Si, the XRD patterns reveal a rather complex microstructure (see Fig. 8). Even though the presence of eta-carbides was prevented in samples with 5.3 wt% C, the XRD pattern
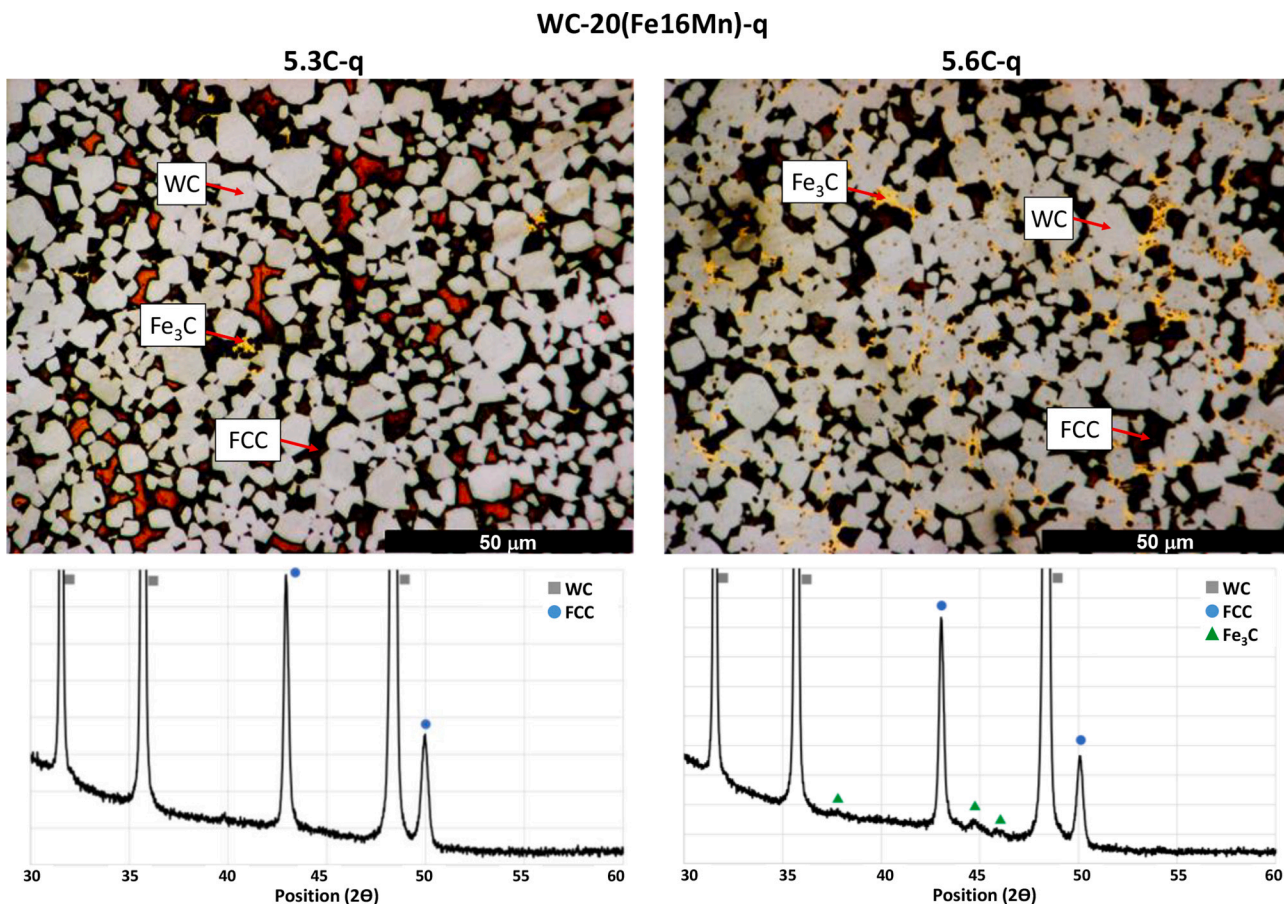
Fig. 5. Quenched alloys WC-20 wt%(Fe16Mn)-q with nominal carbon contents 5.3 wt% C and 5.6 wt%C. X-Ray diffraction patterns and detail of the microstructure after acidic etching with diluted ferric chloride ($FeCl_3$, 5 min.) Red areas in the sample 5.3-q are regions of binder that were not completely eliminated with the acidic etching. (For interpretation of the references to colour in this figure legend, the reader is referred to the web version of this article.)
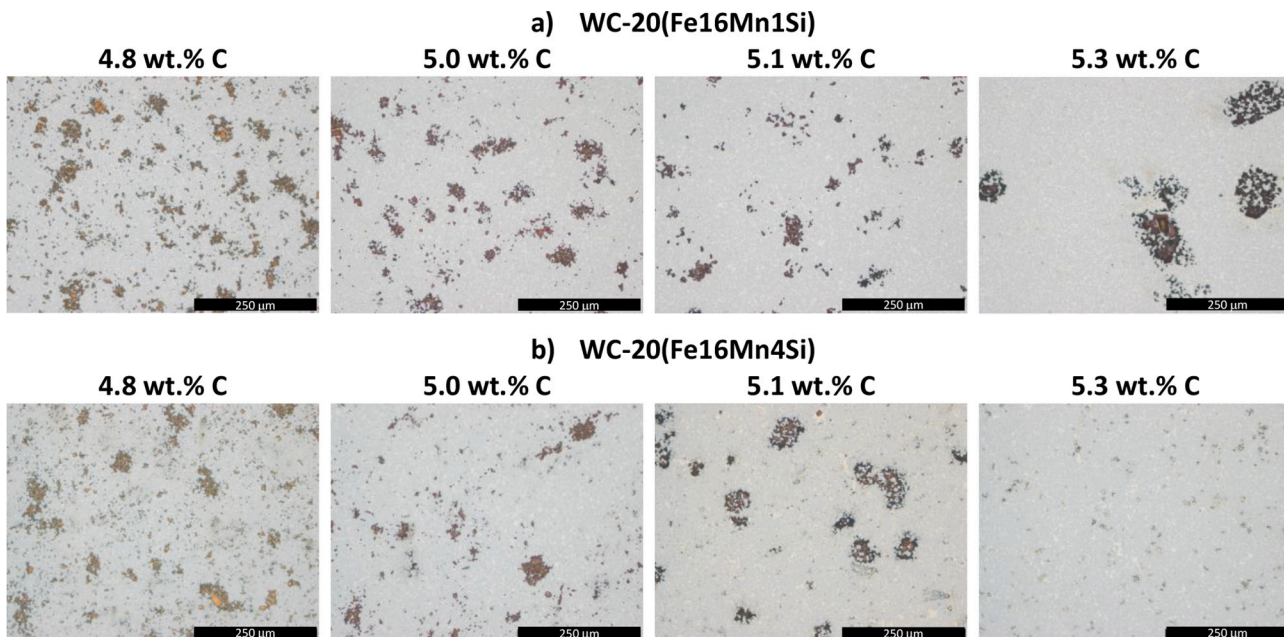

Fig. 6. Alloys WC-20 wt%(Fe16Mn1Si) and WC-20 wt%(Fe16Mn4Si). Microstructures observed experimentally at different nominal carbon contents. Etching: Murakami.
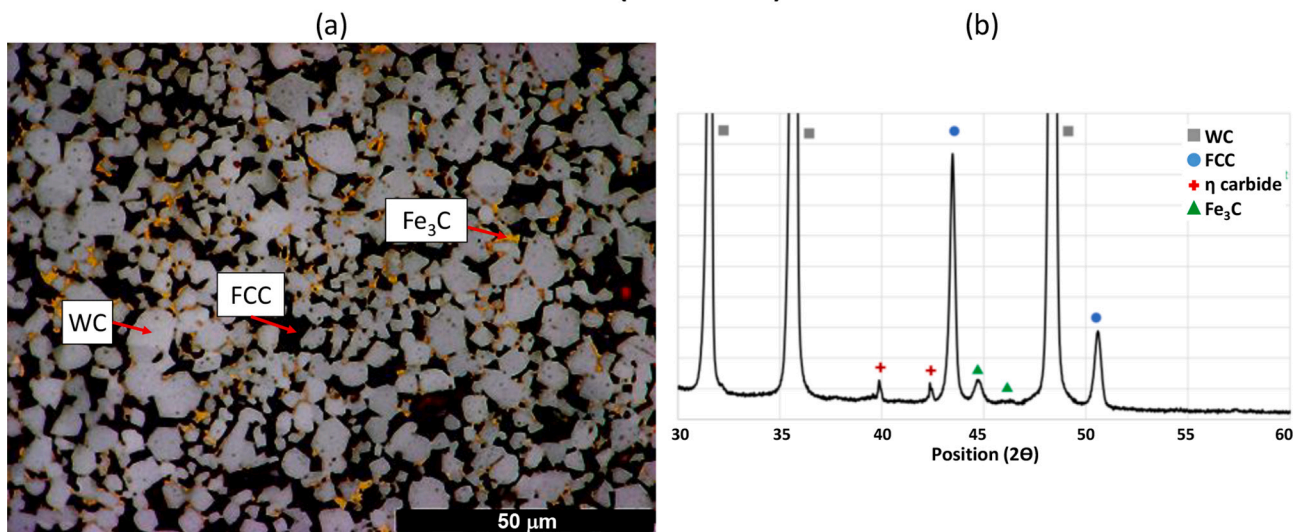
WC-20(Fe16Mn1Si)

Fig. 7. Alloys WC-20 wt%(Fe16Mn1Si) with nominal carbon content 5.3 wt% C. (a) Detail of the microstructure after acidic etching with diluted ferric chloride ($FeCl_3$, 5 min.). (b) X-Ray diffraction pattern.

WC-20(Fe16Mn4Si)

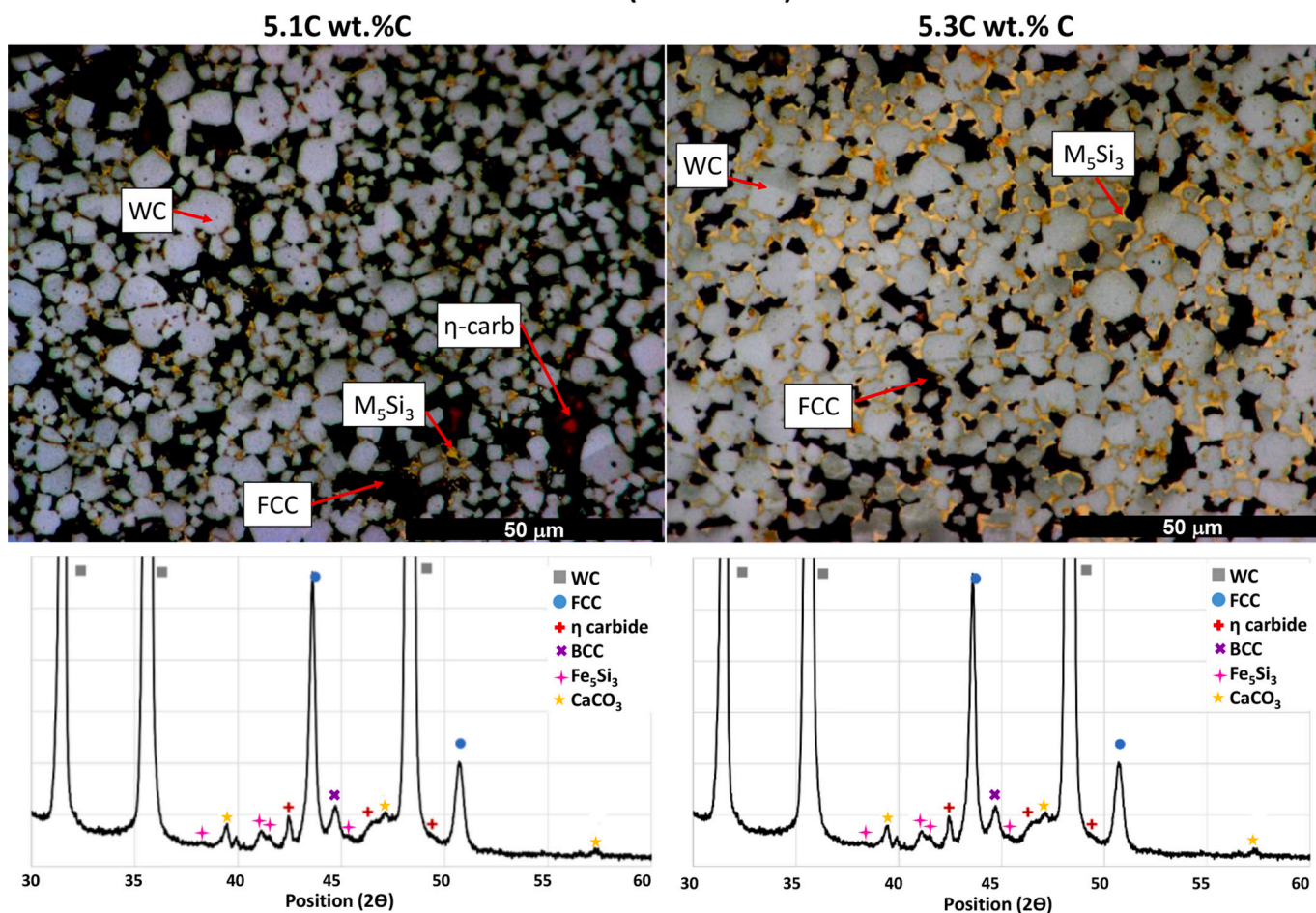### 5.1C wt.%C

5.3C wt.% C

Fig. 8. Alloys WC-20 wt%(Fe16Mn4Si) with nominal carbon contents 5.1 wt% C (left) and 5.3 wt%C (right). X-Ray diffraction patterns and detail of the micro-structure after Murakami etching followed by acidic etching with diluted ferric chloride ($FeCl_3$, 5 min.). η-carbides were clearly identified after etching with Murakami, but after the acidic etching and the adjustment of the image contrast they are difficult to identify in the present image. The $CaCO_3$ pattern detected in the XRD spectra corresponds to the Bakelite resin used to mount the samples for metallographic preparation.

suggest the possible presence of a BCC metallic binder, and also a silicide phase of the type M_5Si_3. The presence of Fe_3C cannot be totally discarded in these samples, because the peaks would overlap with those of the BCC phase. The presence of BCC was confirmed by its second diffraction peak at higher diffraction angles, although it is not depicted in the image. EDX mapping in the alloy Fe16Mn4Si-5.3 wt%C (Fig. 9) revealed the presence of areas enriched in Si, which is consistent with the detection of an M_5Si_3 phase using XRD.

BCC and M_5Si_3 phases also seem to be present in alloys with 5.1 wt% C. The regions identified as M_5Si_3 in Fig. 8 increase as the carbon content increases, and for alloys containing 5.3 wt%C these regions cover almost completely the surface of the WC particles. Specially in the sample with 5.3 wt%C these regions might contain not only M_5Si_3 but also cementite, but the latter one could not be confirmed in any of the samples containing Fe16Mn4Si binders.

3.2.3. Phase formation in Fe25Mn11Ni and Fe22.5Mn25Ni

The evolution in the amount and morphology of eta-carbides in samples containing FeMnNi binders is depicted in Fig. 10.

With 4.9 wt% nominal carbon, Fe25Mn11Ni binders present numerous eta-carbides that are homogeneously distributed in the microstructure(see Fig. 10 -a). In contrast, samples with increasing amounts of nominal carbon (5.2, 5.3 and 5.35 wt%C) present small amounts of dendritically shaped eta-carbides, once again suggesting that these samples might actually be located on the roofed area of the phase diagram. Alloys with 5.4 and 5.6 nominal carbon contents do not show any eta-carbides after etching with Murakami, and they present dense microstructures with no indications of graphite precipitations.

When using a binder with a higher Ni content (Fe22.5Mn25Ni in Fig. 10 -b) the evolution of the microstructure is considerably different. The sample with the lowest nominal carbon content −4.9-clearly shows the presence of eta-carbides, and the next sample in the serie −5.2 wt% C- shows only very few dendritically shaped carbides. In contrast, samples containing 5.3, 5.35 and 5.4 wt%C do not contain eta-carbides and show in general dense and homogeneous microstructures. In this series, the sample with the highest carbon content −5.6 wt%C- shows the typical nest-like graphite porosity.

Further details on the microstructure of these alloys were obtained by combining a short etching time with Murakami (which colors the eta-carbide phases), with an acidic etching (in this case $FeCl_3$), which removes the metallic binder phase. Alloys etched with this procedure are depicted in Fig. 11 (Fe25Mn11Ni alloys) and Fig. 12 (Fe22.5Mn25Ni). It
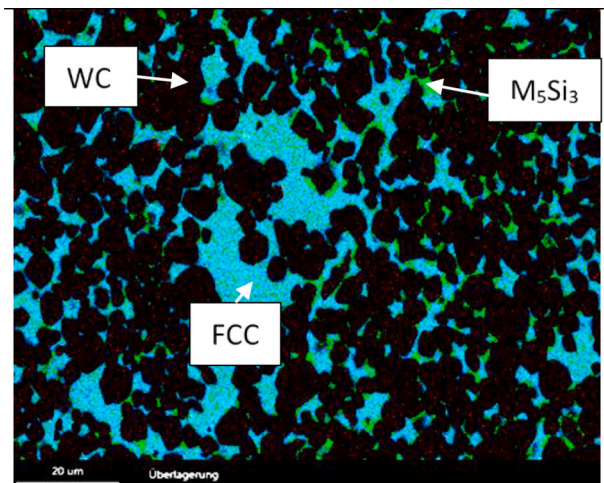

Fig. 9. EDX mapping on alloy Fe16Mn4Si-5.3 wt% C showing green regions that are enriched in Si. These regions have been marked as M_5Si_3 (in accordance with the XRD observations). The binder areas are marked as FCC. (For interpretation of the references to colour in this figure legend, the reader is referred to the web version of this article.)

is clear to see in Fe25Mn11Ni alloys with 5.3 and 5.35 wt% C, that- as in the case of Fe16Mn and Fe16Mn1Si alloys- eta-carbides and cementite (small bright areas in the microstructure) coexist in the microstructure at these carbon contents. Once again, this suggests that there is effectively no "carbon window" in these materials, i.e. it is not possible to obtain microstructures presenting only two phases (WC and metallic binder), independently on the carbon content in the material.

The situation is clearly different when using binders with higher amounts of Ni. As indicated before, alloys with Fe22.5Mn25Ni binders showed no eta-carbides at carbon contents of 5.3 and 5.35 wt% C. As it can be observed in Fig. 12, these sample are also mostly free of cementite phases (only very small cementite ligaments were rarely observed in some areas of the microstructure of samples with 5.35 wt% C). This indicates that these alloys can in fact show two phase microstructures.

Both for Fe25Mn11Ni and for Fe22.5Mn25Ni alloy, samples with 5.4 and 5.6 wt% nominal carbon show cementite phases in the microstructure, demonstrating that, when the solubility of carbon in the binder is exceeded, the first phase stabilized is cementite. While alloys with Fe25Mn11Ni showed no graphite in the microstructure, in Fe22.5Mn25Ni alloys, graphite was stabilized at the highest carbon contents. This does partly agree with the phase diagram, which predicts a stabilization of graphite as the Ni content increases. However, this effect seems to be overestimated in the theoretical diagrams which only predict graphite for Fe22.5Mn25Ni while, in praxis, cementite is also observed with these binders.

4. Discussion

4.1. Phase formation in hardmetals containing FeMn-based binders

Several authors have reported difficulties in obtaining two phase materials when using FeMn-based binders in combination with WC. Prakash used high carbon contents and Hanyaloglu used highly carburizing atmospheres in order to avoid the formation of eta-carbides [16,19]. Maccio observed either eta-carbides or cementite (depending on the carbon content) in all materials produced, concluding that an optimization of the carbon contents needs to be carried out in order to avoid the presence of third phases in the material [20]. In the present work, a detailed examination of the microstructure of hardmetals containing FeMn binders has been carried out following a methodology that combines the use of XRD, SEM + EDS analysis, and selective etching of phases [34,35]. The use of coarse WC powders (6 μm mean size) and relatively high amounts of binder facilitates the observation of phases even when these are present in the microstructure in rather small amounts.

Table 3 summarizes the phases found in the samples produced in this study. WC and FCC were present in all samples, and only the additional phases are indicated in Table 3. It can be clearly seen that none of the samples containing Fe16Mn binders presented a two phase microstructure and, at the intermediate carbon contents (5.3 wt%C), eta-carbides and cementite coexist in the material. In this latter case the eta-carbides present a dendritic morphology which suggests that the samples might have been sintered within the "roofed" region of the phase diagram.

The possibility of avoiding the presence of eta-carbides by a rapid cooling of the samples (quenching) from high temperatures (1370 °C) was investigated. A small piece of the sintered Fe16Mn samples was cut and introduced in a quenching dilatometer where it was rapidly heated up to temperature (~200 °C/s) to avoid carbon losses, and the rapidly cooled with a N_2 gas flow (at ~100 °C/s). By using this procedure the formation of eta-carbides in samples containing 5.3 wt% nominal carbon was avoided, and the binder phase present at room temperature was most likely in a supersaturated state. However, cementite is still present in these samples. Another interesting aspect of the quenched samples is the presence of rather small amounts of a carbidic phase in samples that only presented WC + fcc + η in the sintered state (see Fig. 13). The
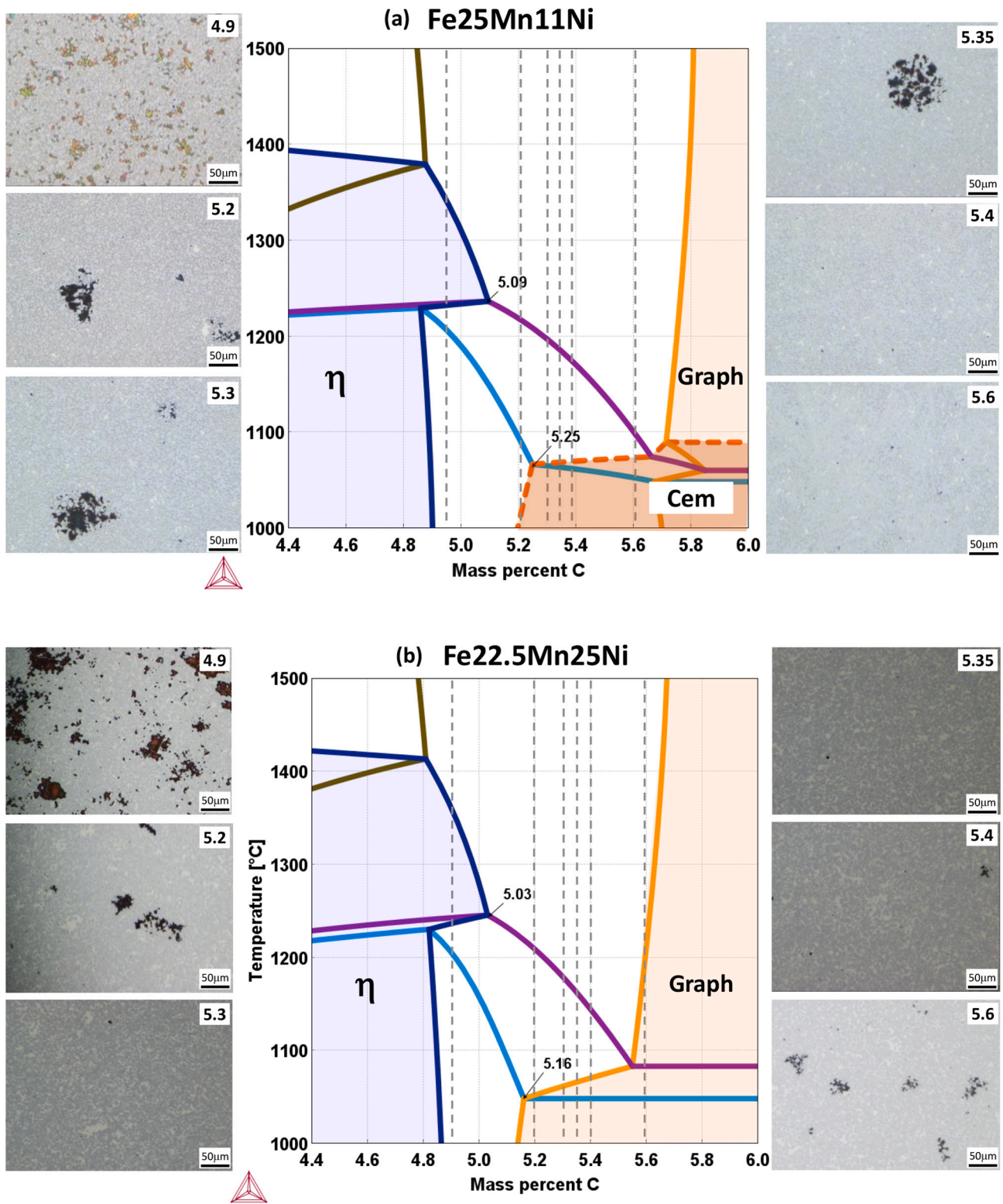
Fig. 10. Alloys (a) WC-20 wt%(Fe25Mn11Ni) and (b) WC-20 wt%(Fe22.5Mn25Ni): Theoretical phase diagram and microstructures observed experimentally at different nominal carbon contents. Etching: Murakami.

simultaneous presence of eta-carbides and cementite in hardmetals containing Fe16Mn binders suggests that, at least under the sintering conditions studied, there is no effective carbon window in this system, and the presence of either eta-carbides or cementite, or both of them, cannot be avoided.

The effectiveness of Si in broadening the carbon window could not be

confirmed experimentally. At 1 wt% Si still an overlapping of eta-carbides and cementite is observed. When increasing the amount of Si to 4 wt%, no eta-carbides were found in samples containing 5.3 wt% carbon or slightly more (5.4 wt%). However, in this case the binder phase does not consist only on an FCC phase, but it might also contain some BCC phase (probably due to the strong stabilization of ferrite
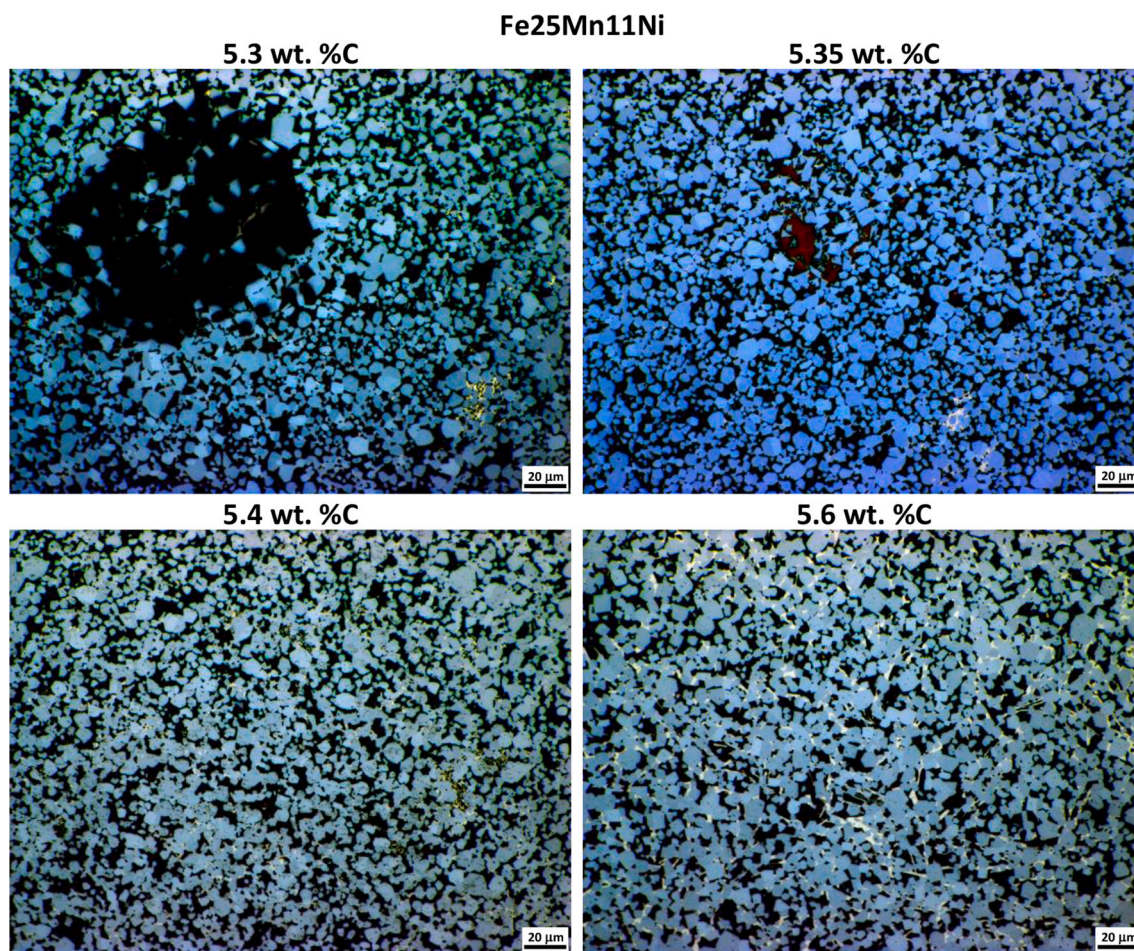
Fig. 11. Alloys WC-20 wt%(Fe25Mn11Ni) with different nominal carbon contents. Detail of the microstructure after acidic etching with diluted ferric chloride (FeCl$_3$, 5 min). Bright spots represent cementite regions (as confirmed by XRD investigations).

caused by Si). Furthermore, most of the samples presented brittle intermetallic phases (most likely M$_5$Si$_3$) that would be most likely detrimental for the toughness of the cemented carbide.

On the other hand, the effectiveness of Ni could indeed be demonstrated. While Fe25Mn11Ni alloys still present a coexistence of eta-carbides and cementite in the microstructure, Fe22.5Mn25Ni samples present two phase materials at 5.3 wt%C, and only very minor amounts of cementite at 5.35 wt% C.

4.2. Binder composition and hardmetal hardness

The composition of the binder phases, as measured by EDS point analysis in coarse binder pools of the microstructure is presented in Table 2. The evolution of the W and Mn content in samples containing increasing amounts of C has been graphically represented in Fig. 14 for different binders.

The highest amounts of W dissolved in the binder are observed in rapidly quenched samples, which contain around 8–10 wt% W, in contrast to the respective as sintered materials that presented W contents below 4 wt%. As suggested by Schubert et al. [5] the low amounts of W in the binder as compared to conventional Co materials (which can dissolve up to ~15 wt%W under normal sintering conditions) can be detrimental for the high temperature properties of these materials. In binders containing 1 wt% Si, the solubility of W in as sintered materials is similar to that observed in Fe16Mn binders, while at 4 wt% Si the W solubility seems to be slightly lower. The lowest W solubility is observed in FeMnNi binders, which is in well agreements with other studies indicating that, when increasing the complexity in the composition of

the binder, the solubility of W is in general decreased [34].

The amount of Mn measured in the binder phase is affected by the W content dissolved, i.e. it will always be lower that the nominal Mn content due to the additional presence of W in the binder of sintered cemented carbides. In general, the Mn contents measured in the binder suggest that there were no relevant Mn losses under the sintering conditions applied in this study: i.e. Mn introduced as masteralloy, moderate sintering temperatures, and N$_2$-H$_2$ flowing atmospheres.

The HV30 hardness of the samples is also represented in Fig. 14 for the different binder compositions. In FeMn and FeMnSi binders no clear trends are observed in the hardnes at increasing carbon contents. Some low carbon samples present rather high hardness values due to the high amounts of eta-carbides in the microstructure, and also the samples with high carbon contents can present rather high hardness values, particularly when high amounts of cementite are observed in the microstructure (i.e. the metallic binder phase is substituted by a harder cementite phase). Also the samples containing 4 wt% Si, for which the presence of cementite could not be confirmed, show relatively high hardness values, which can be explained by the presence of brittle intermetallic phases in the microstructure. Markedly lower hardness values are observed in FeMnNi binders which might partly be a consequence of the considerably lower amounts of cementite observed in these materials. Still, the hardness is comparatively very low as compared with samples containing Fe16Mn or Fe16Mn1Si binders and carbon contents at which the presence of eta-carbides and cementite is relatively low (in particular samples with 5.3 wt% nominal carbon). This might indicate a higher binder hardness in Fe16Mn and Fe16Mn1Si binders, as compared to FeMnNi, which could be affected on one hand by the slightly higher
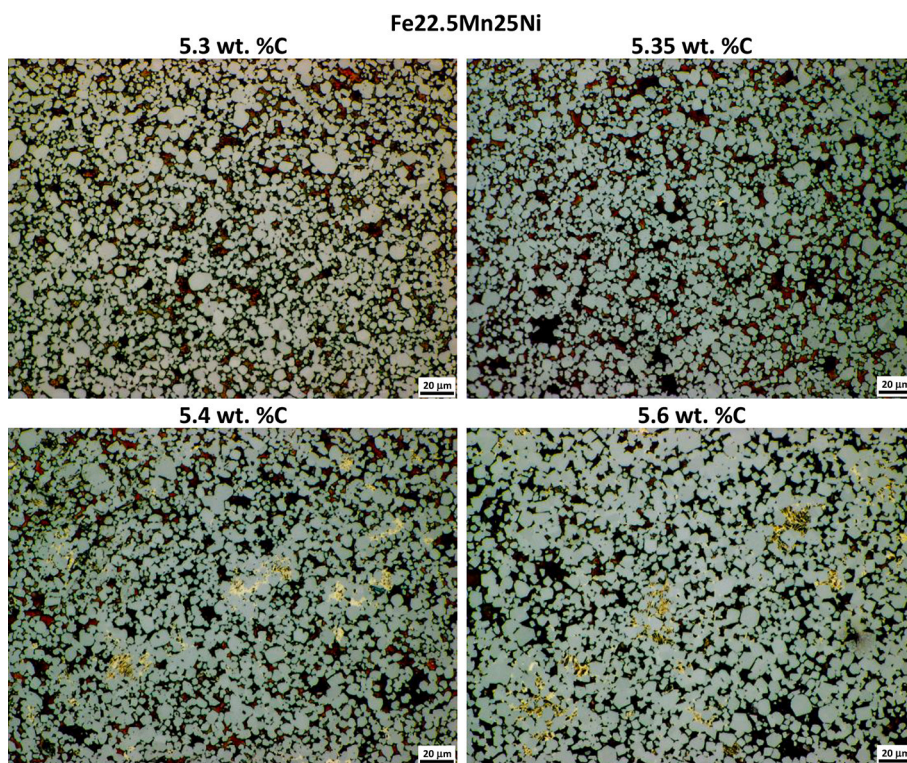
Fig. 12. Alloys WC-20 wt%(Fe22.5Mn25Ni) with different nominal carbon contents. Detail of the microstructure after acidic etching with diluted ferric chloride ($FeCl_3$, 5 min). Bright spots represent cementite regions (as confirmed by XRD investigations).

Table 3
Overview on the phases observed after sintering the alloys considered in this study. The table shows only the phases identified in addition to WC and binder. When no additional phases were found the sample is marked as 2 Phase. Fe_3C marked with * could not be confirmed with XRD or EDX investigations, however, its presence is assumed because a third phase is observed after etching, and the presence of Fe_3C was confirmed at higher carbon contents.

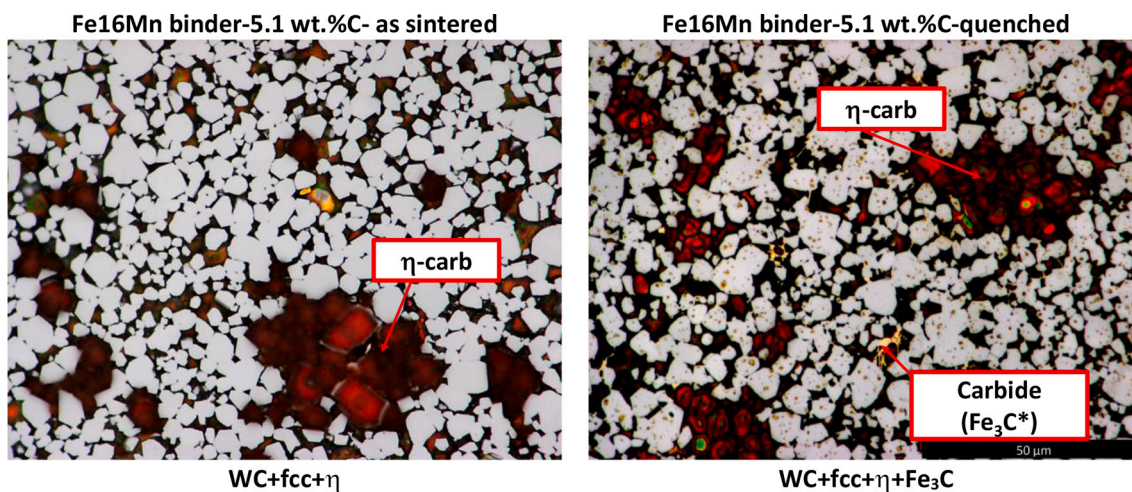| Nominal C (wt%)	4.6	4.8	4.9	5.0	5.1	5.2	5.3	5.35	5.4	5.6
Fe16Mn	η	–	–	–	η	–	η + Fe_3C	–	–	Fe_3C
Fe16Mn(Q)	η	–	–	–	η + (Fe_3C)*	–	Fe_3C	–	–	Fe_3C
Fe16Mn1Si	–	η	–	η	η	–	η + Fe_3C	–	–	–
Fe16Mn4Si	–	η + bcc	–	η + bcc + M_5Si_3	η + bcc + M_5Si_3	–	bcc + M_5Si_3	–	–	–
Fe25Mn11Ni	–	–	η			η	η + Fe_3C	η + Fe_3C	Fe_3C	Fe_3C
Fe22.5Mn25Ni		η	η	η	η	η	**2 Phase**	(Fe_3C)*	Fe_3C	Fe_3C + Graph

Fig. 13. Microstructures of WC-20(Fe16Mn) alloys with 5.1 wt% nominal carbon, in the as sintered state, or after re-heating and quenching from 1370 °C at 100 K/s. The samples were shortly etched with Murakami to colour the eta-carbides, and then etched 5 min with $FeCl_3$ to remove the metallic binder phase.

a)   W content in binder

b)   Mn content in binder
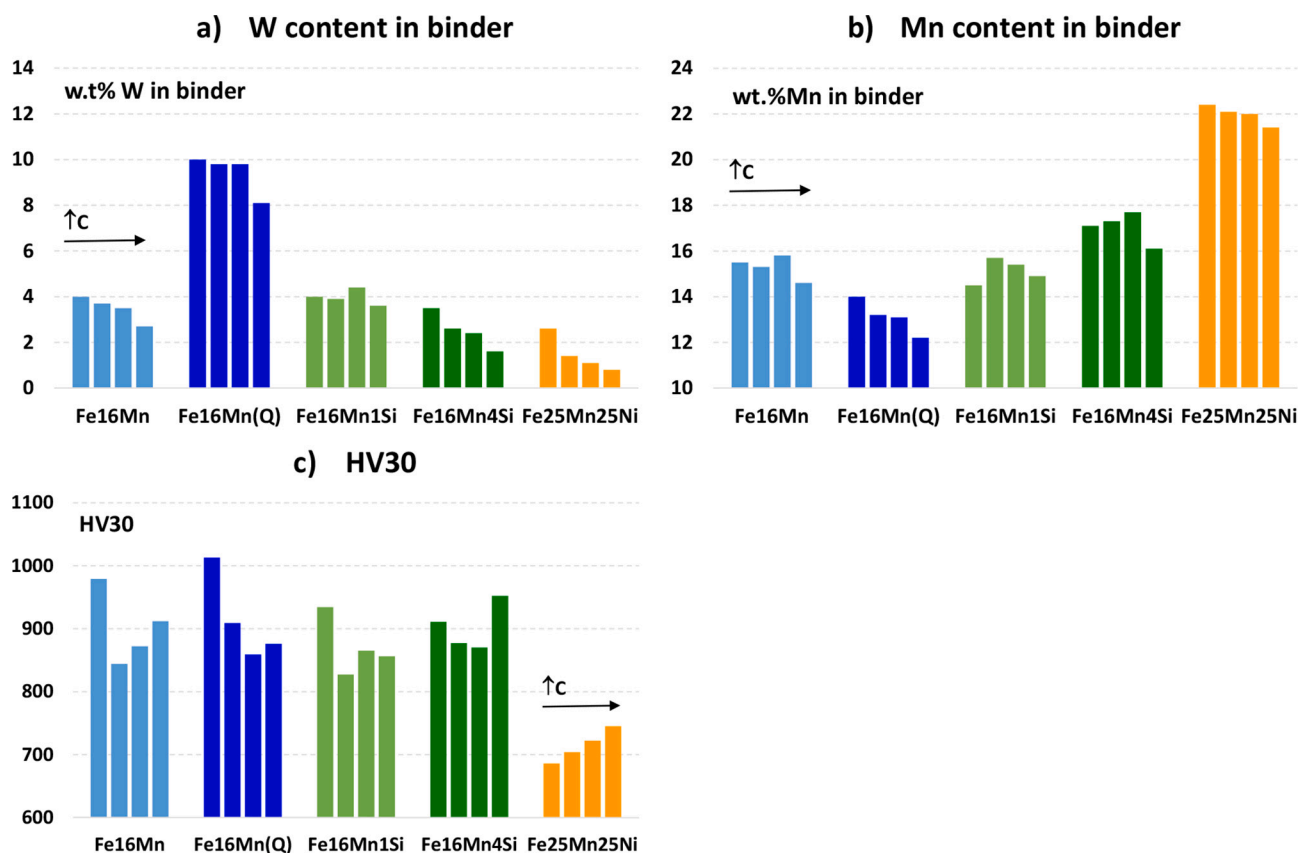

c)   HV30

Fig. 14. Overview on the solubility of Mn (a) and W (b) as well as the hardness HV30 (c) of some of the alloys studied. Different groups correspond to different binder families. Within the same group, 4 carbon contents have been selected going from the minimum (left) to the maximum (right).

dissolution of W, and on the other hand –and probably most importantly- by possible transformation on deformation of Fe16Mn materials, as it is commonly reported for Hadfield steels with similar compositions.

4.3. Oxidation/reduction reactions during sintering

Special care must be taken with the sintering conditions when alloying elements with high oxygen affinity are considered (such as Mn and even more with Si). It is well known from sintered steels that these elements (even in the prealloyed state) may act as internal getters [37,38]. This – in praxis- means that oxidation of these elements can occur even in protective atmospheres with a very low oxygen availability, because the oxygen source is not the atmosphere but the other elements present in the powder mix (in this case WC). Reduction of less stable oxides can then lead to the oxidation of oxygen-sensitive elements such as Mn or Si, this oxygen transference taking place mainly through the gas phase. A proper adjustment of the sintering conditions must be made to ensure the reduction of less stable oxides with H_2 at temperatures at which Mn and Si are still not so avid for oxygen.

In the present study, the introduction of Mn and Si prealloyed in the form of masteralloy particles reduced the oxygen affinity of these elements and thus the risk of oxidation. In any case, a careful selection of the sintering conditions is necessary to avoid phenomena as the "internal gettering effect" [37] or the decarburizing methane formation observed when sintering in H_2 atmospheres [38]. For the optimization of the sintering conditions the application of thermal analysis with the use of mass spectrometry is of outmost importance. In this particular study it was observed how, by a proper adjustment of the sintering conditions, the presence of oxides in the microstructure could be successfully avoided. Fig. 15 demonstrates how, by increasing the holding temperature to 1100 °C, and increasing the sintering temperature to 1380 °C, it

is possible to avoid the formation of oxides on the surface of the masteralloy particles that tend to enclose the masteralloy particles thus inhibiting the distribution of the alloying elements in the microstructure.

4.4. Agreement between experiments and calculations

Thermodynamic calculations could be used to advantage in this study, for estimating the approximate location of the carbon window and thus to make an efficient selection of the carbon contents of interest. It must be stated here that, as the powders were not milled but only mixed, the carbon losses could be approximately estimated from the oxygen content in the starting powders (at least 0.1 wt%). Due to the difficulties for measuring accurately the final carbon content in sintered hardmetals, the results are always expressed in terms of the nominal carbon contents used in the powder mixes. Therefore, when trying to correlate the phase diagrams with the experimentally observed phases it must always be considered that the carbon content in the sintered material will be at least 0.1 wt% lower in carbon than the expressed nominal value. Taking this into account it can be stated that the predictions observed for Fe16Mn and Fe16Mn1Si materials are in rather good agreement with the experimental observations, both in the formation of dendritic eta-carbides under the roofed area, as well as in the presence of cementite instead of graphite at high carbon activities. Another relevant aspect that can be observed in the phase diagrams is the broadening of the region of stability of cementite at low temperatures, at the expense of the two phase region. Further studies would be needed to understand whether this increasing stability of cementite might be at least partly responsible for the coexistence of eta-carbides and cementite in these materials. On the other hand, the predictions observed for Fe16Mn4Si binders cannot be so well related to our
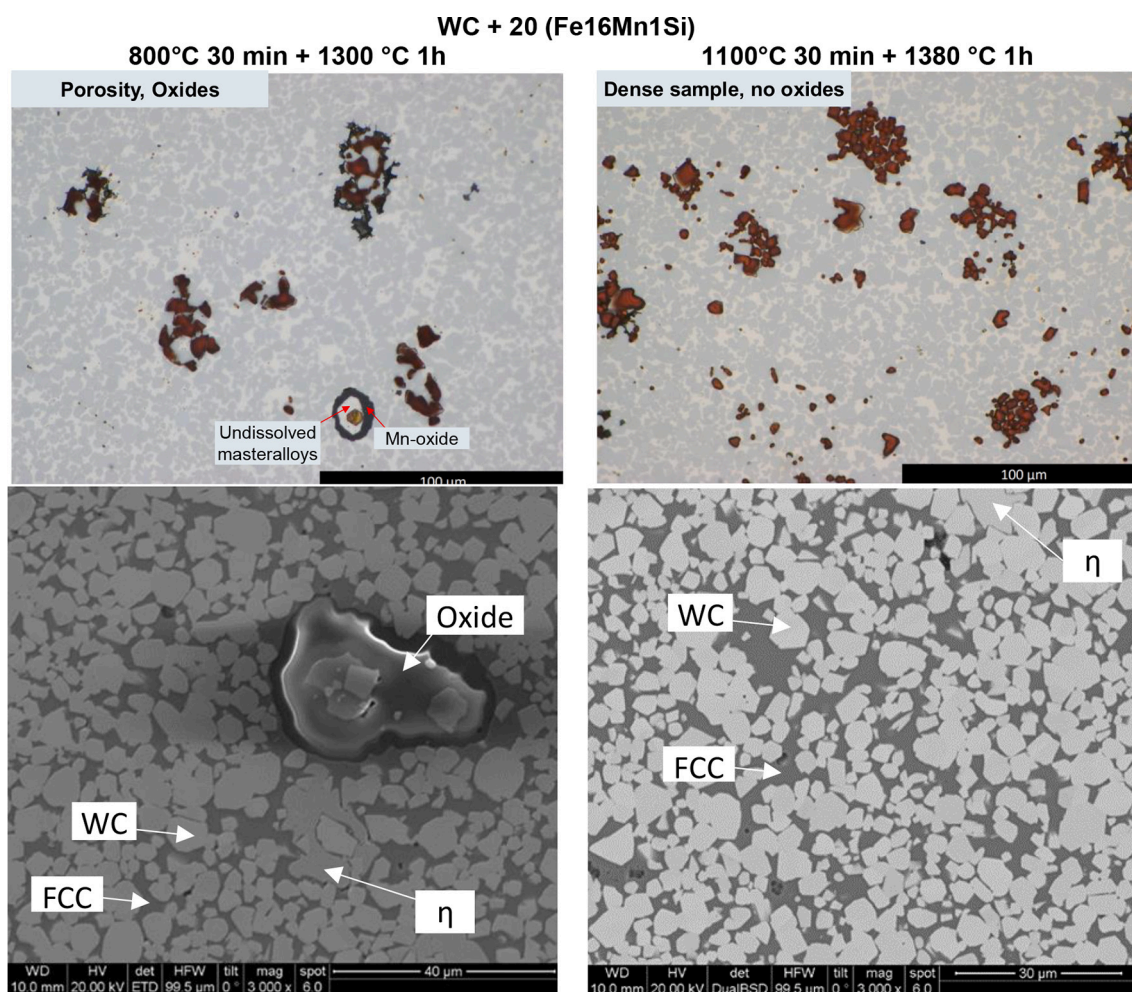
Fig. 15. Microstructure of samples WC-20(Fe16Mn1Si) samples with 5.1 wt%C (nominal). Different sintering conditions are shown at left and right sides.

experiments, mainly because the presence of M_5Si_3 was not predicted in the calculations.

In the case of FeMnNi binders, thermodynamic calculations did again provide a good indication of the carbon contents of interest. The stabilization of cementite at the higher carbon contents was expected from the calculations for the Fe25Mn11Ni binders, but not for the Fe22.5Mn25Ni binders. For the latter ones the software does not predict cementite but graphite. However, the lower stability of cementite in binders with higher Ni contents is evidenced in the samples with the highest carbon (5.6 wt%), for which Fe25Mn11Ni present only cementite, while Fe22.5Mn25Ni binders show both cementite and graphite in the microstructure.

5. Conclusions

When considering the substitution of Co in WC-based cemented carbides, the use of FeMn binders results particularly interesting as these are fully (Co, Ni)- free materials. The available literature suggests that these binders can provide superior hardness, hot hardness or abrasive wear resistance, at the expense of a lower ductility. In this work, phase formation was evaluated for different FeMn-based binders at different carbon contents, with the aim of providing further understanding on the opportunities and challenges faced when considering the substitution of Co with these alternative alloys.

This paper demonstrates that, with the sintering conditions used, it is not possible to obtain two phase materials when using FeMn binders. Due to the efficient stabilization of cementite caused by Mn, either eta-

carbides or cementite are always present in the microstructure. At intermediate carbon contents both phases coexist in the microstructure. Not even the use of very high cooling rates was sufficient to avoid the coexistence of these two phases at the intermediate carbon contents. The formation of cementite might be responsible for the poor ductility reported by other authors for these materials.

Thermodynamic calculations suggest that the addition of Si or Ni to the binder could broaden the carbon window available for the WC-based cemented carbides. At low Si contents this effect was not observed, and at higher Si contents a brittle intermetallic phase (M_5Si_3) was present in the microstructure that was not predicted in the thermodynamic calculations. Only samples with additions of Ni of 25 wt% produced cemented carbides with two phase microstructures. However, the hardness of these materials is significantly lower than that observed with Fe16Mn binders.

Regarding the challenges reported by other authors for avoiding oxide formation and Mn evaporations, it could be proved that the introduction of Mn in a prealloyed form, in combination with a proper adjustment of the sintering conditions, can be used to advantage to achieve a proper sintering of these materials.

Author statement

We hereby declare that all authors have contributed in the realization of this work.

Declaration of Competing Interest

The authors declare that they have no known competing financial interests or personal relationships that could have appeared to influence the work reported in this paper.

Data availability

Data will be made available on request.

Acknowledgements

References

[1] Registration Dossier - ECHA. en-GB, url: https://echa.europa.eu/substance-information/-/substanceinfo/100.028.325, 2023 (visited on 10/08/2023).

[2] K. Schröter, Gesinterte harte Metallegierungen und Verfahren zu ihrer Herstellung, 1923 [DRP 420.689].

[3] Richard Kieffer, Fritz Benesovsky, Hartmetalle de Wien, Springer-Verlag, 1965 isbn: 978-3-7091-8128-7.

[4] L. Prakash, Development of tungsten carbide hardmetals using iron based binder alloys [PhD Thesis], University of Karlsruhe, Germany, 1979.

[5] W.D. Schubert, M. Fugger, et al., Aspects of sintering of cemented carbides with Fe-based binders, Int. J. Refract. Met. Hard Mater. 49 (2015) 110–123.

[6] G. Krauss, Steels - Processing, Structure, and Performance, ASM, Materials Park OH, 2005.

[7] O. Grässel, G. Frommeyer, C. Derder, H. Hofmann, Phase Transformations and Mechanical Properties of Fe-Mn-Si-Al TRIP-Steels, J. Phys. IV Colloque 7 (1997) 383–388.

[8] A.A. Konieczny, On the formability of automotive TRIP steels, in: Proceedings 2003 SAE World Congress 78, SAE International, 2003.

[9] G. Frommeyer, U. Brüx, P. Neumann, Supra-ductile and high-strength manganese TRIP/TWIP steels for high energy absorption purposes, ISIJ Int. 43 (2003) 438–446.

[10] R.A. Hadfield, Hadfield's manganese steel, Science 12 (1888) 284–286.

[11] Y.N. Dastur, W.C. Leslie, Mechanism of work hardening in Hadfield manganese steel, Metall. Trans. A. 12A (1981) 749–759.

[12] P.H. Adler, G.B. Olson, W.S. Owen, Strain hardening of Hadfield manganese steel, Metall. Mater. Trans. A 17 (10) (1986) 1725–1737.

[13] R. Ueji, N. Tsuchida, D. Terada, N. Tsuji, Y. Tanaka, A. Takemura, K. Kunishige, Tensile properties and twinning behavior of high manganese austenitic steel with fine-grained structure, Scr. Mater. 59 (9) (2008) 963–966.

[14] US Patent 4,339,272, Tungsten Carbide-based hard metals, Grover et al, 1982.

[15] L. Prakash, KfK 3374-B, 1983, pp. 50–68.

[16] L.J. Prakash, A note on WC-hardmetals with Fe-Mn binders, in: Herstellung Aufbau (Ed.), Eigenschaften hochschmelzender Verbindungen und Systeme (Hartstoffe und Hartmetalle), Kernforschungszentrum Karlsruhe, Deutschland, 1983, pp. 69–75.

[17] B. Wittmann, PhD Thesis at TU Wien, 2002.

[18] M.R. Maccio, et al., Powder Metall. 55 (2) (2012) 101–109.

[19] C. Hanyaloglu, et al., Mater. Charact. 47 (2001) 315–322.

[20] Maria del Rosario Maccio Colmenares, PhD Thesis at Ruhr-Universität Bochum, 2011.

[21] M. Tarraste, M. Kolnes, J. Kübarsepp, K. Juhani, M. Viljus, J. Külaviir, Green WC-FeMn cemented carbides for industrial wear parts, in: Euro PM2020-Session 22: Alternative HM System Part 2, 2020.

[22] A. Šalak, M. Selecka, Manganese in powder metallurgy steels, Springer-CISP, Cambridge UK, 2012.

[23] A. Salak, Sintered manganese steels part I: effect of structure of initial Iron powders upon mechanical properties, Powder Metall. Int. 12 (1) (1980) 28–31.

[24] A. Salak, Sintered manganese steels part II: manganese evaporation during sintering, Powder Metall. Int. 12 (21) (1980) 72–75.

[25] A. Salak, Sublimation and Condensation of Manganese Vapor, Pract. Metallogr. 22 (1) (1986) 26.

[26] A. Salak, Manganese vapour-protection of premixed manganese steels against oxidation Durinmg sintering, Powder Metall. Int. 18 (4) (1986) 266–270.

[27] A. Salak, Activated Alloying of Fe-Mn Powder Systems by Manganese Vapour during Sintering, Sci. Sinter. 21 (3) (1989) 145.

[28] A. Salak, M. Selecka, R. Bures, Manganese in Ferrous Powder Metallurgy, Powder Metall. Progress 1 (1) (2001) 41–58.

[29] Calderon R. de Oro, M. Jaliliziyaeian, J. Dunkley, C. Gierl-Mayer, H. Danninger, New masteralloys for sintered high strength steels – the attractive route between mixing and prealloying, Powd. Metall. Funct. Coatings 4 (2018) 15–27, https://doi.org/10.17073/1997-308X-2018-4-15-27.

[30] A.F. Guillermet, An assessment of the Fe–Ni–W–C phase diagram, Metallkunde 78 (3) (1987) 165–170 [Bd.].

[31] A.F. Guillermet, Use of phase-diagram calculations in selecting the composition of Fe–Ni bonded WC tools, Int. J. Refract. Met. Hard Mater. (1987) 24–27.

[32] A.F. Guillermet, The Co–Fe–Ni–W–C phase diagram: a thermodynamic descriptionand calculated sections for (Co–Fe–Ni) bonded cemented WC tools, Metallkunde 80 (2) (1989) 83–94 [Bd.].

[33] G.V. Raynor, V.G. Rivlin, Phase Equilibria in Iron Ternary Alloys, The Institute of Metals, London, 1988, pp. 170–171. ISBN 0–901462–34-9.

[34] R. de Oro Calderon, C. Edtmaier, W.-D. Schubert, Novel binders for WC-based cemented carbides with high Cr contents, Int. J. Refract. Met. Hard Mater. 85 (2019) 105063.

[35] de Oro Calderon Raquel, et al., Phase formation in cemented carbides prepared from WC and stainless steel powder–an experimental study combined with thermodynamic calculations, Int. J. Refract. Met. Hard Mater. 80 (2019) 225–237.

[36] V. Lamelas, Rolland M. Bonvalet, M. Walbrühl, A. Borgenstam, Modelling of detrimental phases appearance in cemented carbides, in: Proceedings of Euro PM2021, European Association of Powder Metallurgy, 2021. ISBN: 978-1-899072-54-5.

[37] R. de Oro Calderon, C. Gierl-Mayer, Danninger, Application of thermal analysis techniques to study the oxidation/reduction phenomena during sintering of steels containing oxygen-sensitive alloying elements, J. Therm. Anal. Calorim. 127 (2017) 91–105, https://doi.org/10.1007/s10973-016-5508-5.

[38] R. de Oro Calderon, M. Jaliliziyaeian, C. Gierl-Mayer, et al., Effects of H2 atmospheres on sintering of low alloy steels containing oxygen-sensitive Masteralloys, JOM 69 (2017) 635–644, https://doi.org/10.1007/s11837-017-2287-9.